ISSN 1392 - 1207. MECHANIKA. 2007. Nr.6(68)

Modelling deformable boundary by spherical particle for normal contact

R. Jasevičius*, R. Kačianauskas**
**Vilnius Gediminas Technical University, Saulėtekio al. 11, 10223 Vilnius, Lithuania, E-mail: ma@fm.vgtu.lt*
***Vilnius Gediminas Technical University, Saulėtekio al. 11, 10223 Vilnius, Lithuania, E-mail: rkac@fm.vgtu.lt*

1. Introduction

Among different computational subjects, computational mechanics has probably the longest history of successful development, with its methods having the greatest number of applications. Traditionally, efforts were mainly directed towards macroscopic simulations of various continua and engineering structures.

The progress in computational technologies shifted the efforts towards considering the inside of the material structure on smaller scales. The development of an appropriate numerical research tools for predicting the constitutive behaviour of microstructure is one of the major problems of computational mechanics today. In general, the macroscopic behaviour of continuum is predefined by the structure of grains of various size and shape, or even by individual molecules or atoms. According to the current state of the art, the Discrete Element Method (DEM) is an attractive technique to be applied to modelling of materials at the microscopic level. Here, the term discrete element is considered as synonymous to material particle.

The numerical analysis of any system is performed in the restricted space and is affected by interaction with neighbouring systems. Therefore, the setting up of boundary conditions (BC) is a very important component of mathematical model. The most common types of boundary conditions applied in the framework of DEM simulations are stationary rigid or deformable boundaries. Specification of particular BC concerns various technical details of describing particle-boundary interaction.

Since the appearance of the pioneering work of Cundal and Strack [1] the developments in DEM have been focused on computation models and procedures, basically for modelling and validation of inter-particle contact dynamics, while, investigation of the boundary contacts have received rather limited attention. The earlier study of boundary condition as an interface of granular liquid is given by Allen and Tildesly [2]. The brief reviews of the DEM boundary conditions are also presented by Džiugys and Peters [3] and by Kremmer and Favier [4, 5].

The earliest development, associated with normal linear and nonlinear contacts is given by Allen and Tildesly [2], Briliantov at al. [6] and Džiugys [3], while a recent review of normal contact is given by Kruggel-Emden at al. [7]. Impact behaviour of elastic and elastoplastic spheres has been considered by Wu at al. [8], and inter-particle contact of cohesive powders was studied by Tykhoniuk at al.[9].

The paper addresses the influence of deformability of boundary defined by the variable of particle radius and elasticity modulus. It is organized as follows. The problem of normal particle-boundary contact problem is described in section 2. Equations of motion are presented in section 3. Analytical solution of the linear model is given in section 4, while numerical integration is presented in section 5. Numerical results of the investigation of the Hertz model are presented in section 5, while the conclusions are given in section 6.

2. Particle-boundary contact

The normal noncohesive contact of the elastic spherical particle with the deformable boundary is treated in the conventional manner explored in the DEM. The elastic boundary is also considered as a rigidly fixed spherical particle of variable radius and elasticity modulus.

The normal contact behaviour of a particle with the deformable boundary is investigated by considering a mobile particle bouncing on a horizontal boundary under the influence of gravity. The mobile particle is denoted hereafter by subscript *m,* while the rigidly fixed boundary particle is denoted by subscript *b*. Geometry of the moving particle is defined by constant radius $R_m = const$, while geometry of the boundary particle is defined by variable radius.

Hereafter, the boundary properties are mapped into one-dimensional space of the boundary particle radius measured by relative radius of contacting particles $r = R_b / R_m \ (0.5 \le r \le \infty)$. Here, the lower bound is simply restricted by the value $r = 0.5$, while the upper bound $r = \infty$ presents the half-space in the limit.

The material properties of the particles are assumed to be elastic and defined by Young's modulus *E* and Poisson's ratio ν, while density is ρ. Referring to the above notations, the particles are characterised by E_m and E_b, respectively. Assuming $E_m = const$, the variation of the boundary elasticity properties is characterised by the dimensionless parameter $\zeta = E_b / E_m$, where $(1 \le \zeta \le \infty)$. The limit case $\zeta = \infty$ presents a rigid boundary.

In order to characterize the influence of boundary properties, a series of time histories of the particle bouncing on a deformable boundary will be considered. The study is conducted as follows. The mobile particle is initially located above the boundary with the height H_0. It is subjected to gravitational acceleration *g* pointing in the negative direction *x* and the initial velocity υ_0, if required.

The geometric illustration of the above approach is given in Fig. 1, a, while particular models of the boundary particle are presented in Figs. 1, b-f. Here, the focus is on illustrating the typical boundary models characterized by $0.5 \le r < 1$, $r = 1$ and $r > 1$ (Fig. 1, b-d), and limit

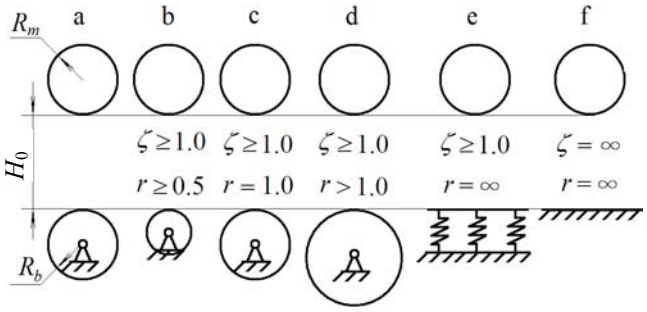

Fig. 1 Illustration of modelling concept (a) and particular boundary models (b-f)

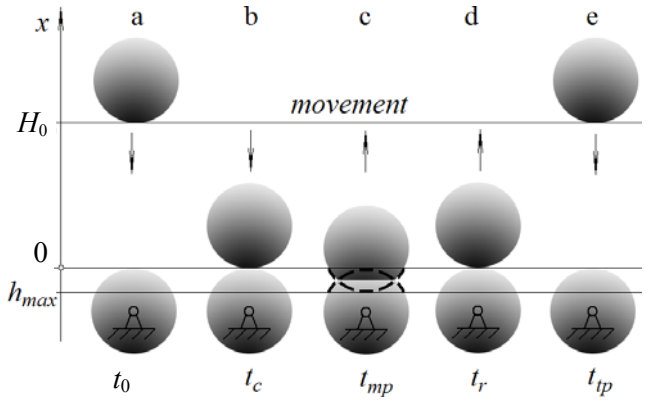

Fig. 2 Characteristic positions of the particles during elastic contact: a - initial state at $t = t_0$, b - initial state of collision at $t = t_c$, c - state of rest (maximum overlap h_{max}) at $t = t_{mp}$, d - rebound $t = t_r$, e - state of maximal rebound height $t = t_{tp}$

cases of elastic and rigid half-space (Fig. 1, e-f).

The illustration of the positions of bouncing particle in time is presented in Fig. 2. When neglecting dissipation, the particle will bounce forever with a constant bouncing period *T*.

The initial location H_0 indicates the distance of the free path between the surfaces of contacting particles. In the case of zero initial velocity $\upsilon_0 = 0$ and initial acceleration a_0 = -g, the initial point corresponds to the highest position of the mobile particle. Let us restrict ourselves to considering of the single bouncing period *T*. A schematic illustration of time histories is given in Fig. 3.

Starting from the initial configuration defined at time instance $t = t_0$ (Fig. 2, a), the particle with constant negative acceleration $g = 9.81\,\mathrm{m/s^2}$ freely moves towards the boundary. At time instance $t = t_c$, the particle having the velocity $\upsilon(t_c) = \upsilon_c$ collides with the boundary (Fig. 2, b). Due to the accumulated energy, the particle penetrates the boundary. It is a conventional assumption that the actual deformation of the colliding particles is replaced by their overlap *h*.

During the contact, the negative velocity of particle reaches the maximum, while the acceleration vector changes direction.

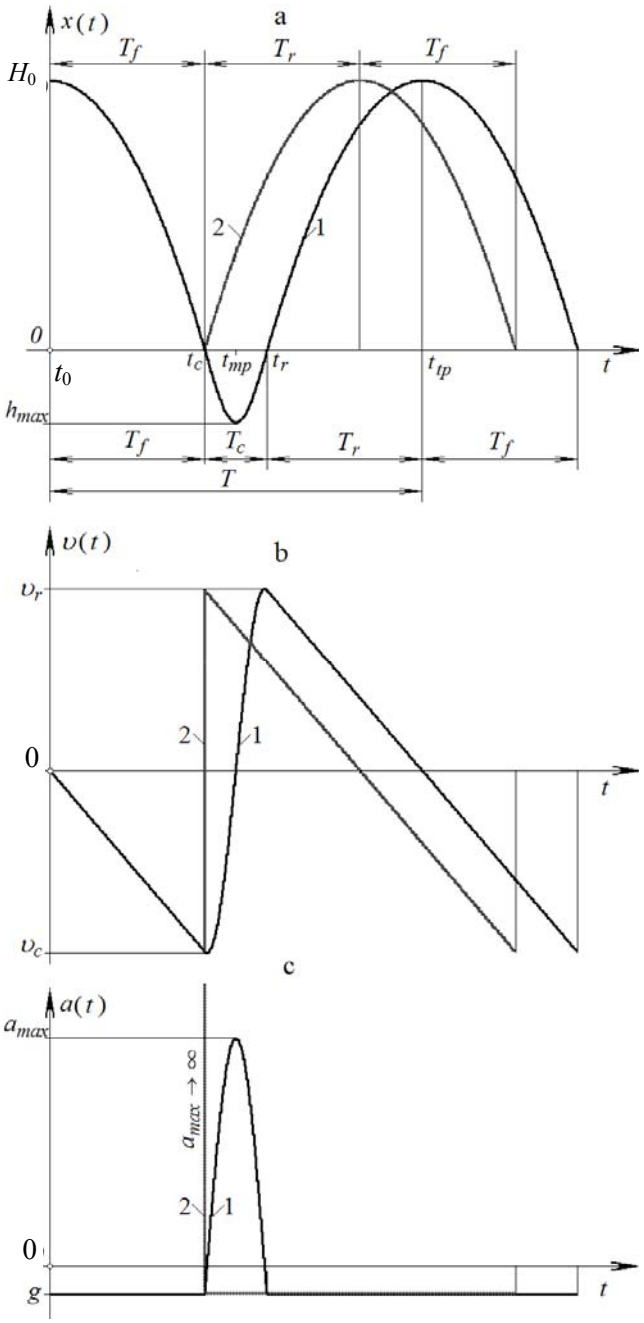

Fig. 3 Schematic time histories of a bouncing particle: a - positions, b - velocities, c - accelerations; *1* - elastic contact; *2* - hard contact

At certain time instance t_{mp}, the mobile particle reaches the state of rest characterized by zero velocity $\upsilon(t_{mp}) = 0$ and the maximum overlap $h(t_{mp}) = h_{max}$ and maximum acceleration $a(t_{mp}) = a_{max}$. After reaching the maximal overlap, the mobile particle starts to move up. At certain time instance $t = t_r$ (Fig. 2, d), the overlap is diminished to zero $h(t_r) = 0$ and, because of the missing of cohesive forces, the particles begins to separate with rebound the velocity $\upsilon(t_r) = \upsilon_r$. Finally, at time instance $t = t_{tp}$, the bounced particle reaches the initial position with velocity $\upsilon(t_{tp}) = 0$.

Thus, the free path of the mobile particle before contact is characterized by the time period $T_f = t_c - t_0$, while the elastic contact lasts for the time period

$T_c = t_r - t_c$. Finally, by taking into account the equality of falling and rising periods $T_r = T_f$, the total period of bouncing is $T = 2T_f + T_c$.

For the sake of comparison the behaviour of the particle in the limit case of rigid boundary is also illustrated by two dashed lines in Fig. 3. Here, the duration of contact reduces to zero $T_c = 0$, thus $t_c = t_r$, while the total bouncing period is $T = 2T_f$. The above simplification used in the event-driven DEM approach yields discontinuous velocity defined as $\upsilon(t_r)$ and undefined value of acceleration $a(t_r)$.

The details of the time history are clearly depicted in Fig. 3, while comprehensive discussion on the normal inter-particle contact model may be found in the book of Pöschel and Schwager [10].

3. Equation of the mobile particle

One-dimensional motion of the bouncing particle *b* defined by position $x(t)$ is described by a classical equation of the second Newton's law. Denoting acceleration as $a(t) = \ddot{x}(t)$, it reads

$$m_m \ddot{x}(t) = F_m(t) \tag{1}$$

where particle mass is

$$m_m = \frac{4}{3}\pi\rho R_m^{\,3} \tag{2}$$

The particle load F_m comprises the gravity force and the elastic contact force. After introducing Boolean variable $\beta_c \equiv \beta_c(t)$, where $\beta_c = 0$ for free particle path and $\beta_c = 1$ for the particle-boundary contact, the loading time history may be presented as follows

$$F_m(t) = -m_m g - \beta_c F_{m,cont}(t) \tag{3}$$

The generalised elastic contact force may be written in terms of the overlap *h*

$$F_{m,cont}(t) = E_{eff} R_{eff}^{2-\alpha} h^{\alpha}(t) \tag{4}$$

where power parameter $\alpha = 1.0$ describes the linear contact model, while $\alpha = 1.5$ is used for the nonlinear Hertz contact model. The effective inter-particle radius and elasticity modulus are as follows

$$R_{eff} = \frac{R_m R_b}{R_m + R_b} \tag{5}$$

$$E_{eff} = \frac{4}{3}\frac{E_m E_b}{E_m\left(1-\nu_i^2\right) + E_b\left(1-\nu_j^2\right)} \tag{6}$$

Taking into account the dimensionless notations *r* and ζ, the effective parameters may be expressed in terms of parameters of the mobile particle. The effective radius is

$$R_{eff} = \frac{rR_m}{r+1} \tag{7}$$

Assuming equal Poisson's ratios $\nu = \nu_i = \nu_j$, the effective elasticity modulus may be expressed as

$$E_{eff} = \frac{4}{3}\frac{\zeta E_m}{(1+\zeta)\left(1-\nu^2\right)} \tag{8}$$

By substituting (3)-(8), the equation of particle motion (1) may be rewritten as follows

$$\ddot{x}(t) + \beta_c p^2 x^{\alpha} = -g \tag{9}$$

here, the parameter is

$$p = \sqrt{\frac{E_{eff} R_{eff}^{2-\alpha}}{m_m}} \tag{10}$$

After simple rearrangement of Eq. (10), we get

$$p = \bar{p} c R_m^{(-1-\alpha)/2} \tag{11}$$

where

$$c = \sqrt{\frac{E_m}{\rho}} \tag{12}$$

is the material constant. The non-dimensional parameter is

$$\bar{p} = \sqrt{\frac{1}{\pi}\frac{\bar{\zeta}(\bar{r})^{2-\alpha}}{\left(1-\nu^2\right)}} \tag{13}$$

where

$$\bar{r} = \frac{r}{r+1};\ \bar{\zeta} = \frac{\zeta}{\zeta+1} \tag{14}$$

The contact equation contains the parameters of contacting particles. The initial conditions defined at the initial time $t_0 = 0$ contain initial position H_0 and velocity υ_0

$$\begin{cases} x\big|_{t=0} = H_0 \\ \dot{x}\big|_{t=0} = \upsilon_0 \end{cases} \tag{15}$$

Since Eq. (9) contains a discontinuous term, the additional continuity conditions have to be imposed on the velocities at contact and rebound instances t_c and t_r, respectively

$$\begin{cases} \dot{x}^-\big|_{t=t_c} = \dot{x}^+\big|_{t=t_c} \\ \dot{x}^-\big|_{t=t_{tp}} = \dot{x}^+\big|_{t=t_{tp}} \end{cases} \tag{16}$$

In the case of the instantaneous rigid contact, occurring at time instance $t_c = t_r$, the discontinuity condition reads as

$$\dot{x}^{+}\Big|_{t=t_c} = -\dot{x}^{-}\Big|_{t=t_c} \tag{17}$$

The above defined relationships (15)-(16) yield some additional conditions required for proper tracking of the particle motion.

4. Solution technique

4.1. Numerical time integration scheme

The dynamic state of the mobile particle is determined by numerical integration of Eq. (9) with initial and continuity conditions (15)-(16). Generally, in the presence of the nonlinear terms, the problem must be solved numerically. Reviews and comprehensive discussions on integration methods applied in DEM simulations may be found in the works [2, 3, 11]. In order to find a reasonable compromise between accuracy and computational efficiency, explicit one-step or predictor–corrector integration schemes prevail. Generally, it was observed that higher order schemes exhibited higher accuracy. In the latest investigations Roughier [11] revealed, however, a tendency of higher-order schemes to be more sensitive to instabilities, though not necessarily computationally efficient. On the basis of numerical experience, the *5*th – *order Gear predictor-corrector* scheme [2] was employed in n numerical simulations.

This predictor-corrector scheme represents a two-step procedure. Let us denote the time-dependent variables, positions $x(t)$, velocities $\upsilon(t) = dx/dt$, accelerations $a(t) = d^2x/dt^2$ as well as the higher-order time derivatives $b_3(t) = d^3x/dt^3$, $b_4(t) = d^4x/dt^4$ and $b_5(t) = d^5x/dt^5$ of the particle by vector $\mathbf{y} = \{x, v, a, b_3, b_4, b_5\}^T$. The new value variables at time increment $t+\Delta t$ are predicted by a simple series expansion up to a desired order of accuracy

$$\mathbf{y}^p(t+\Delta t) = \mathbf{y}(t) + \Delta\mathbf{y}^p(\Delta t) \tag{18}$$

Here, the incremental vector $\Delta\mathbf{y}^p(\Delta t)$ presents the required terms of the expansion series. Then, according to the new positions and velocities, the particle forces and accelerations are corrected and acceleration increment Δa is updated. Finally, the vector of particle variables is corrected as follows

$$\mathbf{y}^c(t+\Delta t) = \mathbf{y}^p(t+\Delta t) + \Delta\mathbf{y}^c(c_j, \Delta t, \Delta a) \tag{19}$$

Here, the correction vector $\Delta\mathbf{y}^p$ is calculated by using the given integration constants c_j.

A detailed description of DEM technique applied may also be found in Balevičius at al. [12].

4.2. Validation test

The performance of the explicit integration scheme (18)-(19) and the choice of the time increment Δt have to be validated. The most common way to validate numerical tool is to compare integration results with analytical solution. In the considered problem, defined by Eq. (9), only the free particle path, when $\beta_c = 0$, and a linear case of contact model when $\beta_c = 1.0$ and $\alpha = 1.0$, may be solved analytically, respectively.

Generally, a path of the bouncing particle presents a periodic function with the period T, applied by the integer number n ($n = 1, 2, 3,\ldots$) of periods, or simply of contacts. Logically, the particle motion may be characterized by its time intervals t^*, t^{**}, t^{***}.

The first time interval of the free-falling particle t^* is defined by a half of the free-path period $0 < t^* < 0.5T_f$. The time interval of the elastic contact t^{**} may be defined as $(n-0.5)T_f + (n-1)T_c < t^{**} < (n-0.5)T_f + nT_c$, while time interval between contacts t^{***} is defined as $(n-0.5)T_f + nT_c < t^{***} < (n+0.5)T_f + nT_c$.

Tracing of bouncing particle comprises time-histories of positions $x(t)$, velocities $\dot{x}(t)$ and accelerations $\ddot{x}(t)$. The explicit solution of the Eq. (9) for the free path of the particle [3, 12-14] and for linear contact model [3, 12-14] may be defined as follows. It reads for positions as

$$\begin{cases} x(t^*) = H_0 - 0.5gt^2 & \text{(a)} \\ x(t^{**}) = p^{-2}\left(\upsilon_c p\, sin(pt) + g(cos(pt) - 1)\right) & \text{(b)} \\ x(t^{***}) = -\upsilon_c t - 0.5gt^2 & \text{(c)} \end{cases} \tag{20}$$

for velocities as

$$\begin{cases} \dot{x}(t^*) = -gt & \text{(a)} \\ \dot{x}(t^{**}) = \upsilon_c\, cos(pt) - \dfrac{g}{p} sin(pt) & \text{(b)} \\ \dot{x}(t^{***}) = -\upsilon_c - gt & \text{(c)} \end{cases} \tag{21}$$

and for accelerations as

$$\begin{cases} \ddot{x}(t^*) = -g & \text{(a)} \\ \ddot{x}(t^{**}) = -g - \left(\bar{p}^2 c^2 R_m^{-1-\alpha}\right) x(t) & \text{(b)} \\ \ddot{x}(t^{***}) = -g & \text{(c)} \end{cases} \tag{22}$$

A detailed description of the particle motion may be made in explicably in terms of characteristic parameters, which may be exposed in tests.

On the basis of the free motion solutions (20, a-21, a), the free motion period is

$$T_f = \sqrt{2H_0 g^{-1}} \tag{23}$$

while collision velocity is expressed as

$$\upsilon_c = -\sqrt{2H_0 g} \tag{24}$$

On the basis of the contact motion solutions (20-

22, b) the main contact parameters T_c, h_{max}, υ_c and a_{max} are extended. When $x(t_{mo}) = h_{max}$, the following maximum acceleration from (22, b)

$$a_{max} = -h_{max} p^2 - g \tag{25}$$

By considering maximum overlap conditions $\dot{x}(t_{mo}) = 0$, the contact period may be obtained from (21, b) as

$$T_c = 2p^{-1} arctan(\tau) \tag{26}$$

where

$$\tau = |\upsilon_c| p g^{-1}$$

It should be noted, that, under appropriate conditions, when $r \geq 1.0$, $\zeta \geq 1.0$ and $H_0 \geq R_m$, $arctan(\tau) \approx \pi / 2$.

A formula for the contact period can also be found in Džiugys at al. [3]. For practical purposes explicit expressions are given in terms of stiffness and mass. In this case the formula (26) for the above contact period is closed to a popular simplified expression, see [3]

$$T_c = \pi p^{-1} \tag{27}$$

In time t_{mo}, the penetration is maximum. By substituting (26) in to (20, b) maximum overlap value can be calculated as follows

$$h_{max} = -\frac{\sqrt{\upsilon_c^2 p^2 - g^2} + g}{p^2} \tag{28}$$

A formula for maximum overlap can also be found in Džiugys at al. [3]

$$h_{max} = \upsilon_c p^{-1} \tag{29}$$

Following the existing practice, the time integration step has to be a fraction of the contact period $\Delta t = \eta T_c$, where scaling factor η varies usually in the range of 1/10 and 1/50. It is well known that the investigation of hard particles requires the application of a smaller integration step. Therefore, relatively hard boundary particles defined by $r = 100$ and by $\zeta = 100$ were employed for validation. The mobile particle with $c^2 = 1 \cdot 10^7$ and $\nu = 0.3$ was chosen. Other data were chosen as follows: $R_m = 0.5$ mm, $H_0 = 5R_m$, $\upsilon_0 = 0$. The collision velocity obtained according to (21) is υ_c = -0.313 m/s. The contact parameters h_{max}, a_{max} and υ_c, as well as the rebound time t_r, were considered as quality indicators after the second contact.

Two values of η_1 and η_2 were examined in order to validate the numerical integration scheme by tracking the complete particle path up to the second ($n = 2$) rebound. For the linear model, the contact period obtained by expressions (26) yield $T_{cL} = 848.3$ns. Thus, assuming $\eta_1 = 1/10$ and $\eta_2 = 1/50$ we get the values of integration steps $\Delta t_1 = 85$ ns and $\Delta t_2 = 1.7$ ns.

The numerical results obtained for the linear model based on different time Δt_1 and Δt_2 steps along with analytical solution and percentage differences δ_1 and δ_2 are presented in Table 1.

For the nonlinear model, the contact period is described, by these expressions (Brilliantov at. al.) [6]

$$T_c = 2.94 \left(\frac{m_{eff}}{k} \right)^{2/5} \left(\upsilon_c \right)^{-1/5} \tag{30}$$

where

$$k^2 = \left(\frac{4}{5} \frac{2}{3\Lambda} \right)^2 R_{eff}; \; \Lambda = \frac{2E_1 + 3E_2}{E_1 (E_1 + 6E_2)} \tag{31, a}$$

$$E_1 = \frac{E_m}{1 + \nu}; \; E_1 = \frac{nE_m}{1 + \nu} \tag{31, b}$$

The contact period obtained by (30) yields $T_{cN} = 4.29$ μs. Thus, assuming the same fractions $\eta_1 = 1/10$ and $\eta_2 = 1/50$, we get two values of integration steps $\Delta t_1 = 0.429$ μs and $\Delta t_2 = 85$ ns. The numerical results for the non-linear Hertz model and percentage difference δ are presented in Table 2.

Table 1

The results of validation test for linear model

	t_r, ms	h_{max}, nm	a_{max}, nm/ms^2	υ_r, m/s
Δt_1	96.59	-86.4	118.6	0.319
Δt_2	96.0	-85.0	116.6	0.315
Analyt.	95.8	-84.6	116	0.313
δ_1 %	0.825	2.1	2.24	1.84
δ_2 %	0.209	0.473	0.517	0.562

Table 2

The results of validation test for Hertz model

	t_r, ms	h_{max}, nm	a_{max}, nm/ms^2	υ_r, m/s
Δt_1	96.45	-532	239	0.316
Δt_1	95.8	-524	234	0.313
δ %	0.678	1.53	214	0.958

The numbers given in Table 1 show that minimal time step Δt_1 leading up to 2% errors may be insufficient for long particle path. The numbers in Table 2 obtained by nonlinear model illustrate the same tendency. Finally, contact time step fraction $\eta_2 = 1/50$ will be further applied in numerical solutions.

5. Simulation results

The above-mentioned bouncing particle model (9)-(14) was explored for the simulation of normal particle-boundary contact in order to determine the influence of the boundary properties. Analytical expressions (20)-(29)

were used for the solution of the linear model, while the numerical *5*th – *order Gear predictor-corrector* time integration scheme (18)-(19) was used for the solution of nonlinear Hertz contact model.

The simulation of contact was performed by using previously defined data, while the relative radius r and elasticity modulus ζ are retained as modelling variables.

Simulation results in the form of time histories of overlap h are plotted in Fig. 4. The overlap displacements are normalised and presented by dimensionless variables as $h^*(t) = h/h_{NL\_max}$.

The value scaling parameters $h_{NL\_max} = 0.521\,\mu m$ and $T_{c\_NL} = 4.896\,\mu s$ respond to the stiffest case of Hertz contact, yielding $T_c^* = 1.0$ and $h^*(t) = 1.0$. This case is manifested as numerically achievable limit indicating rigid boundary.

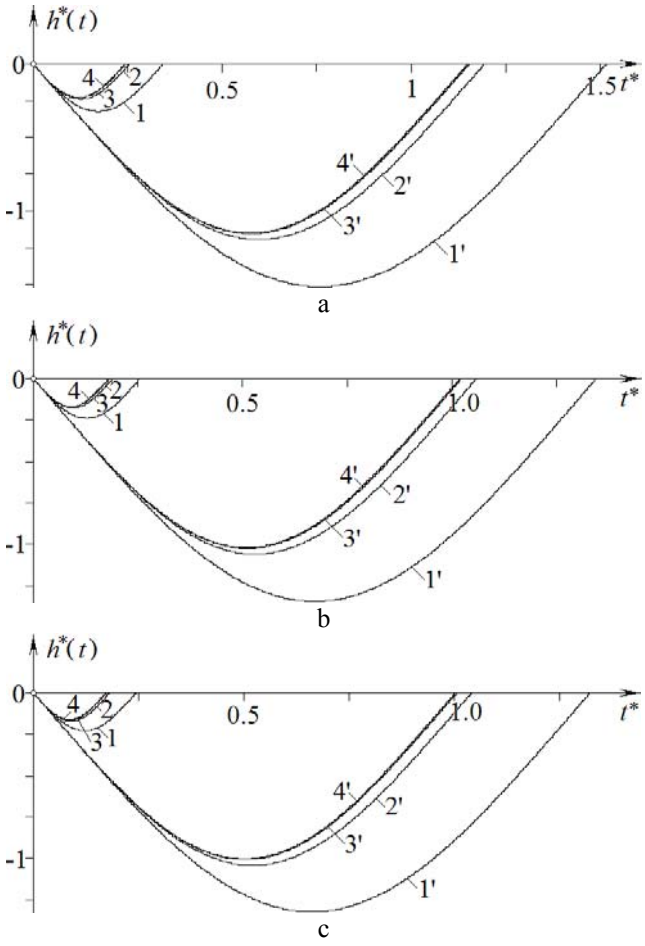

Fig. 4 Time histories of overlap displacement: a - $r_1 = 1.0$; b - $r_2 = 10$; c - $r_3 = 100$

Here, Fig. 4 present the results for different values of relation radii defined by $r_1 = 1.0$, $r_2 = 10$ and $r_3 = 100$ respectively. Each figure contains the results of linear as well as nonlinear models, while each of the four curves 1, 2, 3 and 4 represents the results for various elasticity modulus of boundary particle, i.e. $\zeta_1 = 1.0$, $\zeta_2 = 10$, $\zeta_3 = 100$ and $\zeta_4 = 1000$ respectively.

It would be of interest to note that the limit overlap displacement h_{NL_max} indicates 0.104% overlap for mobile particle and $0.104 \cdot 10^{-3}$% overlap for boundary particle, which really proves the assumption of the rigid boundary.

Convergence of inter-particle contact behaviour to particle-plane, or half-space behaviour may be better explained by considering variation of the relative maximum overlap $h_{max}^* = h_{max}/h_{NL\_max}$ and scaled by the previously defined parameter h_{NL}. Variation of $h_{max}^*(r)$ against the relative inter-particle radius r is plotted in Fig. 5. Here, each of the four curves 1, 2, 3 and 4 represents the results for various relative elasticity module of boundary particle, i.e. $\zeta_1 = 1.0$, $\zeta_2 = 10$, $\zeta_3 = 100$ and $\zeta_4 = 1000$ respectively.

Variation of $h_{max}^*(\zeta)$ against the relative elasticity modulus is plotted in Fig. 6. Here, each of the four curves 1, 2, 3 and 4 represents the results for various relative radii of boundary particle, i.e. $r_1 = 0.5$, $r_2 = 1.0$, $r_3 = 10$, $r_4 = 100$ and $r_5 = 1000$ respectively.

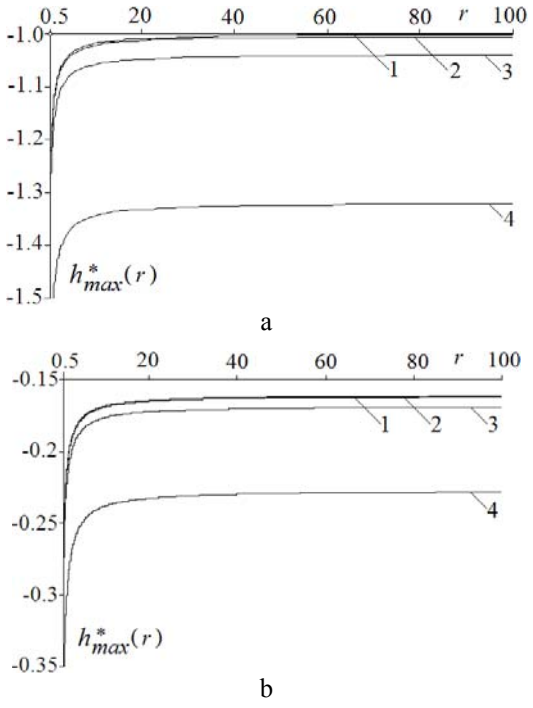

Fig. 5 Variation of overlap displacement against inter- particle radius: a - linear model, b - Hertz model

It was clearly observed that stiffening of the boundary by increasing both radii or elasticity modulus of the boundary particle has stabilisation tendency for overlap displacement. This tendency is also held for other contact parameters, including contact period T_c, maximum acceleration a_{max} and rebound velocity υ_r. Variation of contact period $T_c^* = T_c/T_{c\_NL}$, duration against the particle elasticity modulus for the case of linear model is presented in Fig. 7 as an illustration by Hertz model.

From the above graphs it can be easily observed when increasing r and ζ, the relative value diminishes and approaches a negligibly small value in the limit. This may be explained as the convergence of the value to a rigid boundary. Convergence rate would be better illustrated quantitavely by introducing new relative variables, playing the role of the error indicators.

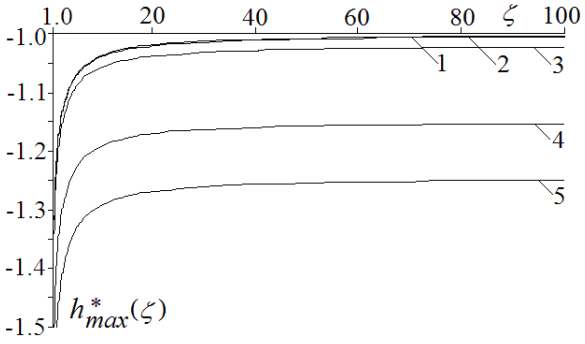

a

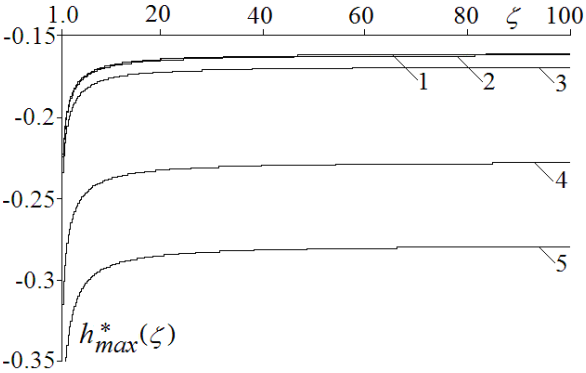

b

Fig. 6 Variation of overlap displacement against the particle elasticity modulus: a - linear model, b - Hertz model

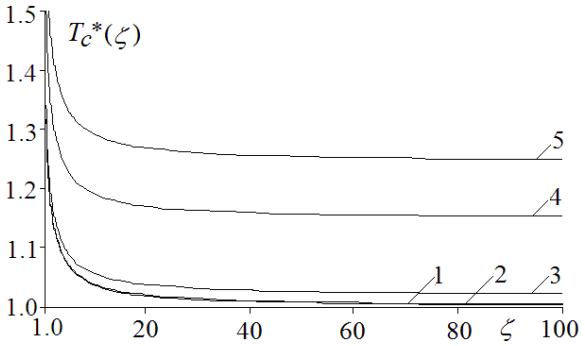

a

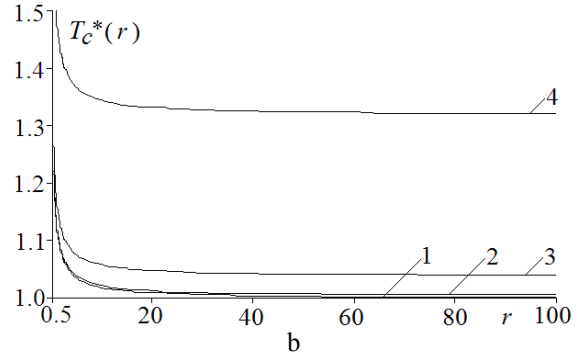

b

Fig. 7 Variation of contact period displacement against the particle: a - elasticity modulus and b - radius in Hertz model

Variations of the inter-particle displacement curves depicted in Fig. 6 against elasticity modulus are checked by indicator (32, a), while the results of this rate transformation are plotted in Fig. 8, a. Variation of theoretical indicator (33, a) is also presented for the sake of comparison. The results show that all curves independently of both linear and Hertz contact models are transformed to a single curve. The curve illustrates that the variation of indicator in the range from 10 to 100 yields the difference 4.829% in linear model and 3.845% in Hertz model, while the variation of indicator in the range from 100 to 1000 decreases only up to the difference of 0.4485% (linear) and 0.359% (Hertz). On the base of the above indication it is easy to conclude that relative elasticity modulus of the boundary $\zeta = 100$ may be considered as a limit value applicable for practical DEM simulation purposes. Convergence of the linear as well as Hertz contact models with respect to increased elasticity modulus of the boundary is of the type $\zeta^{-1/2}$.

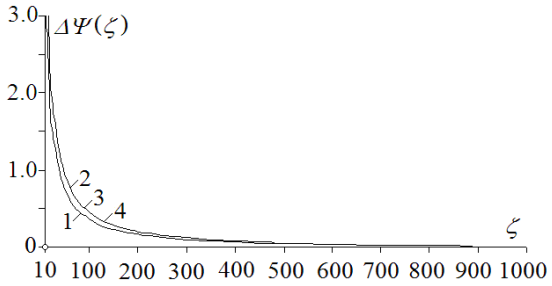

a

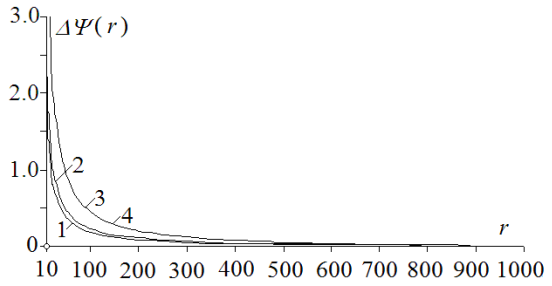

b

Fig. 8 Variation of contact period indicator against the particle: a - elasticity modulus and b - radius. *1* - Hertz numerical; *2* - Hertz theoretical; *3* - linear numerical; *4* - linear theoretical

Extending simulation range to $r_{max} = 1000$ and $\zeta_{max} = 1000$, the rate indicators are defined as

$$\Delta\Psi_{num}(\zeta) = 100\left(h(\zeta) - h(\zeta_{max})\right)/h(\zeta_{max}) \qquad (32, a)$$

$$\Delta\Psi_{num}(r) = 100\left(h(r) - h(r_{max})\right)/h(r_{max}) \qquad (32, b)$$

Additionally, two theoretical indicators in nonlinear model are expressed in the following way

$$\Delta\Psi_{th}(\zeta) = 100\bar{\zeta}_{\max}^{\,1/2}\left(\bar{\zeta}^{\,-1/2} - \bar{\zeta}_{\max}^{\,-1/2}\right) \qquad (33, a)$$

$$\Delta\Psi_{th}(r) = 100\bar{r}_{\max}^{\,(2-\alpha)/2}\left(\bar{r}^{\,(\alpha-2)/2} - \bar{r}_{\max}^{\,(\alpha-2)/2}\right) \qquad (33, b)$$

are introduced. Where

$$\bar{\zeta}_{\max} = \frac{\zeta_{\max}}{\zeta_{\max}+1};\ \bar{r}_{\max} = \frac{r_{\max}}{r_{\max}+1}$$

Variations of all curves depicted in Fig. 5 against particle radius are checked by indicator (32, b), while the results of this rate transformation are plotted in Fig. 8, b in the above manner. Variations of theoretical indicator (33, b) $\Delta\Psi_L(r)$ and $\Delta\Psi_H\left(r^{2-\alpha}\right)$ responding to two different values of α are also added. The results show that all curves of linear and Hertz contact models are transformed to two curves. The curve of Hertz model illustrates that the variation of indicator in the range from 10 to 100 yields 1.904% difference, while the variation of indicator in the range from 100 to 1000 decreases only up to 0.179% difference.

The indicator of the linear model is actually the same as in previous case. On the basis of the above indication, it can be concluded that, in spite of the slight difference observed in contact model, relative radius of the boundary particle $r = 100$ may be considered as a limit value. Convergence of contact models with respect to the increased radius is of the type $\overline{r}^{(\alpha-2)/2}$.

6. Conclusions

The performed investigation of boundary particles may be generalised in the following manner. It was found, that basic particle contact parameters, such as contact duration, maximum overlap, maximum acceleration and rebound velocity, converges to the appropriate limits with respect to the increased elasticity modulus and particle radius of the boundary. Convergence of all parameters with respect to the increased relative elasticity modulus ζ of the boundary is of the type $\sqrt{(\zeta+1)/\zeta}$, while convergence with respect to the relative boundary radius r of the particle is predefined by model dependent power factor α and is of the type $\sqrt{((r+1)/r)^{2-\alpha}}$. For practical DEM simulation purposes, the above limits may be defined by the values $\zeta = 100$ and $r = 100$. The recommendations provided could be useful for the simulation of the boundary particles applied in the DEM simulations.

References

1. **Cundall, P.A., Strack, O.D.L.** A discrete numerical model for granular assemblies. -Geotechnique, 1979, v.29, No1, p.47–65.
2. **Allen, M.P., Tildesley, D.J.** Computer Simulation of Liquids.-Oxford: Clarendon Press, 1991.-385p.
3. **Džiugys, A., Peters**, **B.J.** An approach to simulate the motion of spherical and nonspherical fuel particles in combustion chambers.-Granular Matter 3. Springer – Verlag, 2001, p.231-266.
4. **Kremmer, M. and Favier, J.F.** A method for representing boundaries in discrete element modelling – part I: Geometry and contact detection.-Int. J. for Numerical and Analytical Methods in Geomechanics, 2001, v.51, p.1407-1421.
5. **Kremmer, M. and Favier, J.F.** A method for representing boundaries in discrete element modellig – part II: Kinematics. -Int. J. or numerical and analytical methods in geomechanics, 2001, v.51, p.1423-1436.
6. **Brilliantov, V., Spahn, F. & Hertzsch, J.M., Pöschel, T.** Model for collisions in granular gases. -Physical Review, 1996, v.53, No5, p.5381-5393.
7. **Wu, C.-Y., Li, L.-Y., Thornton, C.** Energy dissipation, during normal impact of elastic and elastic-plastic spheres.-Int. J. of Impact Engineering, 2005, v.32, p.593-604.
8. **Tykhoniuk, R., Tomas, J., Luding S., Kappl, M., Lars, H., Butt, H.J.** Ultrafine cohesive powders: From interparticle contacts to continuum behaviour. -Chemical Engineering Science. -Elsevier, 2007, v.62, p.2843-2864.
9. **Kruggel-Emden, H., Simsek, E., Rickelt, S., Wirtz, S., Scherer, V.** Review and extension of normal force models for the Discrete Element Method.-Powder Technology.-Elsiever, 2007, v.171, p.157-173.
10. **Pöschel, T. & Schwager, T.** Computational Granular Dynamics.-Berlin: Springer–Verlag, Heidelberg, 2005. -322p.
11. **Rougier, E., Munjiza, A. & John, N.W.M.** Numerical comparison of some explicit integration schemes used in DEM, FEM/DEM and molecular dynamics. -Int. J. Numerical Methods Engineering, 2004, v.61, p.856-879.
12. **Balevičius, R., Kačianauskas, R., Džiugys, A., Maknickas, A., Vislavičius, K.** DEMMAT code for numerical simulation of multi-particle dynamics. -Information Technology and Control, 2005, v.34. No1, p.71-78.
13. **Balevičius, R., Džiugys, A., Kačianauskas, R.,** Discrete element method and its application to analysis of penetration into granular media.-J. of Civil Engineering and Management, 2003, p.3-14.
14. **Žiliukas, P., Barauskas, B.** Mechanical Vibrations. -Kaunas: Technologija, 1997.-310p.

R. Jasevičius, R. Kačianauskas

DEFORMUOJAMO KONTŪRO MODELIAVIMAS SFERINE DALELE, ESANT NORMALINIAM KONTAKTUI

R e z i u m ė

Straipsnyje diskrečiųjų elementų metodu (DEM) nagrinėjamas tamprios sferinės dalelės normalinis kontaktas su deformuojamu pagrindu. Nustatyto spindulio dalelė juda veikiama sunkio jėgos. Deformuojamas kontūras nagrinėjamas kaip įtvirtinta kintamo tamprumo modulio ir kintamo spindulio sferinė dalelė. Ribinis atvejis – kai pagrindo spindulys artėja į begalybę ir atspindi tampruįį puserdvį, o didinant tamprumo modulį pagrindas atitinka kietąją dalelę. Tiesinis modelis ir netiesinis Herco kontakto modelis, taikant diskretinių elementų metodą, tiriami skaitiškai, naudojantis 5-osios tikslumo eilės prediktoriaus-korektoriaus Giro integravimo schema. Skaitinio modelio tiesinis atvejis testuojamas lyginant su analitiniu sprendiniu. Nagrinėjama dalelės padėtis, greitis ir pagreitis. Remiantis modeliavimo rezultatais nustatytos pagrindo dalelės ribinės reikšmės ir pateiktos rekomendacijos dėl deformuojamojo kontūro rodiklių pasirinkimo modeliuojant DEM.

R. Jasevičius, R. Kačianauskas

MODELING DEFORMABLE BOUNDARY BY SPHERICAL PARTICLE FOR NORMAL CONTACT

S u m m a r y

The normal contact of the elastic spherical particle with deformable boundary is investigated in terms of the Discrete Element Method (DEM). The particle of the prescribed radius is moving under gravity and the initial velocity. The deformable boundary is treated as rigidly fixed spherical particle with variable elasticity modulus and variable radius. The limit case, approaching the infinite radius presents an elastic half-space, while increasing of the elasticity modulus presents the rigid boundary, respectively.

The linear model and the nonlinear Hertz contact model used in the discrete element method are investigated numerically by applying the 5th-order Gear's predictor-corrector integration scheme. The numerical model is tested by comparing it with analytical solution. The time variations of the particle positions, velocities and accelerations are presented. On the basis of simulation results the limit values of the boundary particle parameters are evaluated and recommendations for the boundary particle parameters required in DEM simulation are drown.

P. Ясявичюс, P. Качянаускас

МОДЕЛИРОВАНИЕ ДЕФОРМИРУЕМОЙ ГРАНИЦЫ СФЕРИЧИСКОЙ ЧАСТИЦЕЙ ПРИ НОРМАЛЬНОМ КОНТАКТЕ

Р е з ю м е

В рамках метода дискретных элементов в (МДЭ) рассматривается упругий нормальный контакт сферической частицы с деформируемой границей. Частица предписанного радиуса перемещается под действием гравитационной силы. Деформирующая граница рассматривается как стационарная сферическая частица с переменным модулем упругости и переменным радиусом. Приближение радиуса частицы к бесконечности представляет предельный случай упругого полупространства, а приближение модуля упругости к бесконечности – жесткую границу. Линейная и нелинейная модель Герца, используемая МДЭ, применяется для моделирования нормального контакта. Задача контакта решена численно, применяя для интегрирования уравнений движения схему 5-го ряда Гира. Численно исследованы положения скорости и ускорения частицы. На основе результатов моделирования исследованы предельные параметры границы и предложены рекомендации по выбору рациональных параметров граничной частицы для моделирования МДЭ.

Received September 24, 2007